

A De-Embedding Method Using Different-Length Transmission Lines for mm-Wave CMOS Device Modeling

Naoki TAKAYAMA^{†a)}, Kota MATSUSHITA^{†b)}, Shogo ITO^{†c)}, Nonmembers,
Ning LI^{†d)}, Student Member, Keigo BUNSEN^{†e)}, Nonmember, Kenichi OKADA^{†f)},
and Akira MATSUZAWA^{†g)}, Members

SUMMARY This paper proposes a de-embedding method for on-chip S-parameter measurements at mm-wave frequency. The proposed method uses only two transmission lines with different length. In the proposed method, a parasitic-component model extracted from two transmission lines can be used for de-embedding for other-type DUTs like transistor, capacitor, inductor, etc. The experimental results show that the error in characteristic impedance between the different-length transmission lines is less than 0.7% above 40 GHz. The extracted pad model is also shown.

key words: de-embedding, S-parameter measurement, mm-wave, RF CMOS, transmission line

1. Introduction

Recently, the research on mm-wave CMOS circuits becomes a hot topic [1], [2]. CMOS processes are employed for developing mm-wave wireless systems because of the low cost fabrication comparing with compound semiconductors [3]. In mm-wave circuits, even small parasitic capacitors and inductors will considerably affect the total circuit performance. Therefore, it is needed to build accurate models of the components including parasitic elements, such as transistors, capacitor, transmission line, and so on.

Before building models of them, the process, de-embedding, is needed to remove parasitic components from measurement data because measurement data include the parasitic components of the contact pads. A variety of de-embedding methods for on-chip measurement have been proposed [4], [5]. There is one of the most common methods called open-short method [6]. The method, however, cannot remove parasitic components of the contact pads completely in high frequency because it is difficult to fabricate an ideal short pattern.

Some de-embedding methods using only line patterns without short pattern were proposed [7]–[9]. One of them uses a thru pattern [7]. However, the measurement result of the thru pattern has a large uncertainty and is not reliable because the value of the S-parameter is too small.

The length of thru pattern must be short because the measurement data is converted to a π -type lumped-component circuit. On the other hand, too short thru-pattern causes larger measurement error. According to the probe manufacturer (Cascade Microtech, Inc.), RF probes should be separated more than 200 μm . Too close probes have larger interference, and it results in larger measurement error [10]. Thus, the de-embedding result is also not reliable. The de-embedding method using only long line patterns is proposed in [8]. However, this method considers only the shunt parasitic component of the contact pads and the series parasitic component are ignored. Moreover, this method is only applicable to de-embedding of a transmission line, not for other test element groups. In addition, there is a de-embedding method using two transmission lines [9], and the method is evaluated up to 110 GHz with experimental results using a 60 GHz power amplifier [11]. However, the method in [9] has the limitation that one transmission line has to be exactly twice as long as the other.

The new technique proposed in this paper can remove not only the shunt parasitic components of the pads but also the series one by using two transmission lines with different length [12]. In addition, this method can be applied to other test element groups, such as transistors, capacitors, and so on, by building a model of the contact pads.

2. Conventional Methods

2.1 Open-Short De-Embedding

At first, we introduce Open-Short De-embedding noted above [6]. This method builds the model of the contact pads and the ground plane, as shown in Fig. 1, from the measurement data of an open pattern and a short pattern. The equivalent circuits of the patterns are shown in Fig. 2. The shunt parasitic components (Y_{P1} , Y_{P2} , Y_{P3}) are removed from the measurement data by subtracting the Y-parameter

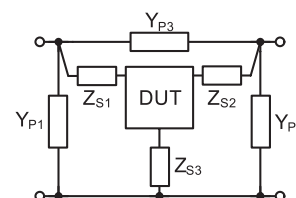


Fig. 1 Equivalent circuit used in the open-short de-embedding.

Manuscript received October 14, 2009.

Manuscript revised January 20, 2010.

[†]The authors are with the Department of Physical Electronics, Tokyo Institute of Technology, Tokyo, 152-8552 Japan.

- a) E-mail: takayama@ssc.pe.titech.ac.jp
 - b) E-mail: matsushita@ssc.pe.titech.ac.jp
 - c) E-mail: itos@ssc.pe.titech.ac.jp
 - d) E-mail: lining@ssc.pe.titech.ac.jp
 - e) E-mail: bunsen@ssc.pe.titech.ac.jp
 - f) E-mail: okada@ssc.pe.titech.ac.jp
 - g) E-mail: matsui@ssc.pe.titech.ac.jp
- DOI: 10.1587/transle.E93.C.812

of the open pattern. As the same procedure, the shunt parasitic components of a short pattern can be removed. Therefore, the matrix consisting of only series parasitic components (Z_{S1} , Z_{S2} , Z_{S3}) is obtained. By subtracting this matrix, the matrix of the DUT is obtained.

However this method has an issue at high frequencies like mm-wave frequency. It is impossible to fabricate ideal open and short patterns due to parasitic capacitance and inductance, and the non-ideality causes considerable degradation in the de-embedding accuracy, especially at the mm-wave frequency.

2.2 Thru-Only De-Embedding

Next, we introduce the thru-only de-embedding [7]. Fig. 3 shows the structure of a transmission line and the equivalent circuit of the measurement data. This method uses only a short thru pattern. Figure 4 shows the structure of a short thru and the equivalent circuit. The π -type equivalent circuit is utilized to characterize the measurement data. The pad model is built by separating the equivalent circuit into two symmetric parts.

However, this method has an issue. The length of the short thru has to be as short as possible because the equivalent circuit consists of lumped components. However, if the length is short, the distance between the probes is too close. Therefore, the measurement data become poorly-reproducible and unreliable.

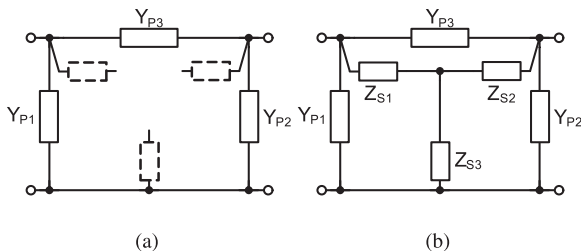


Fig. 2 Equivalent circuits. (a) Open pattern. (b) Short pattern.

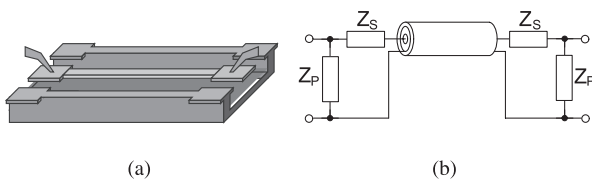


Fig. 3 Transmission line. (a) Structure. (b) Equivalent circuit.

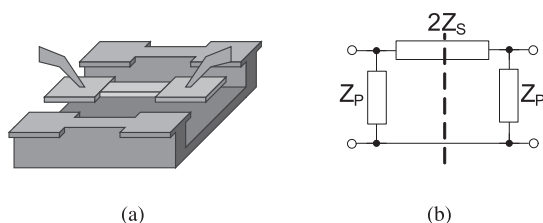


Fig. 4 Short thru. (a) Structure. (b) Equivalent circuit.

3. Proposed Method

3.1 Multi-Line De-Embedding

As explained in the previous sections, the conventional open-short and thru-only methods are not so accurate at mm-wave frequencies, which is caused by the non-ideality of open- and short-patterns and the inaccuracy of the short thru pattern. Thus, this paper proposes a novel de-embedding method using two long line patterns [12]. In this method, first the transmission line is characterized by using the measurement data. The parasitic components of the contact pads are calculated and the pad model is built. The structure of the contact pad and the equivalent circuit are shown in Fig. 5. The circuit consists of 4 components and the values of them are frequency dependent. The pad model built by two transmission lines can be utilized to de-embed the pad parasitics of other-type DUTs such as transistors, capacitors, inductors, etc. The procedure of the proposed method is as follows.

3.2 De-Embedding Procedure

Before building the model of the contact pads, the transmission line has to be characterized. Measurement data of two transmission lines with a length of ℓ_1 and ℓ_2 , where $\ell_1 < \ell_2$, are used in this method. While the method in [9] requires the condition $\ell_2 = 2\ell_1$, the proposed method can utilize various length of transmission lines. Separating the segments of contact pads from the intrinsic line, the T-parameter matrix of test structure ℓ_i , $\mathbf{T}_{\ell_i}^m$, can be expressed by the following equation.

$$\mathbf{T}_{\ell_i}^m = \mathbf{T}_{PL} \cdot \mathbf{T}_{\ell_i} \cdot \mathbf{T}_{PR}, \quad (1)$$

where

\mathbf{T}_{ℓ_i} represents the T-parameter of the intrinsic line ℓ_i , \mathbf{T}_{PL} represents the T-parameter of the left pad, and \mathbf{T}_{PR} represents the T-parameter of the right pad.

Subsequently \mathbf{T}_{X1} is defined as multiplying $\mathbf{T}_{\ell_2}^m$ by the inverse of $\mathbf{T}_{\ell_1}^m$ (Fig. 6).

$$\begin{aligned} \mathbf{T}_{X1} &= \mathbf{T}_{\ell_2}^m \cdot [\mathbf{T}_{\ell_1}^m]^{-1} \\ &= \mathbf{T}_{PL} \cdot \mathbf{T}_{\ell_2} \cdot \mathbf{T}_{PR} \cdot \mathbf{T}_{PR}^{-1} \cdot \mathbf{T}_{\ell_1}^{-1} \cdot \mathbf{T}_{PL}^{-1} \end{aligned}$$

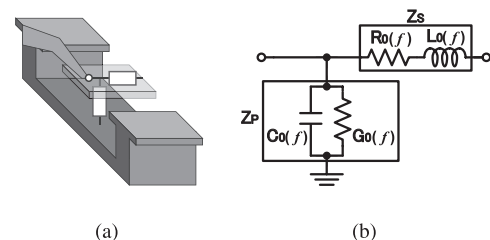


Fig. 5 Contact pad model. (a) Structure. (b) Equivalent circuit.

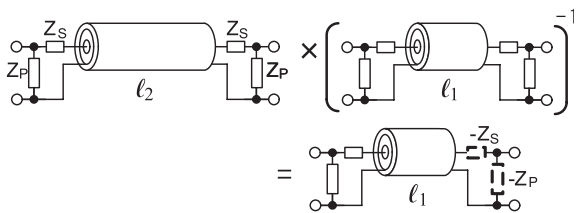


Fig. 6 Multiplying the matrices of the transmission line.

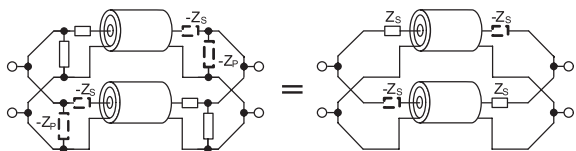


Fig. 7 Canceling the pad parasitic Z_P .

$$= \mathbf{T}_{PL} \cdot \mathbf{T}_{l_1} \cdot \mathbf{T}_{PL}^{-1} \quad (2)$$

T-parameter of this matrix \mathbf{T}_{X1} is transformed to the Y-parameter matrix \mathbf{Y}_{X1} . A parallel combination of \mathbf{Y}_{X1} and a port-swapped version of itself, $\text{Swap}(\mathbf{Y}_{X1})$, is defined as \mathbf{Y}_{X2} . Thus, we can cancel the effect of the pad parasitic Z_P as shown in Fig. 7.

$$\begin{aligned} \mathbf{Y}_{X2} &= \mathbf{Y}_{X1} + \text{Swap}(\mathbf{Y}_{X1}) \\ &= \begin{bmatrix} Y_{X1,11} & Y_{X1,12} \\ Y_{X1,21} & Y_{X1,22} \end{bmatrix} + \begin{bmatrix} Y_{X1,22} & Y_{X1,21} \\ Y_{X1,12} & Y_{X1,11} \end{bmatrix} \end{aligned} \quad (3)$$

\mathbf{Y}_{X3} is defined as the Y-parameter matrix of the intrinsic TL connected with the pad series parasitic component Z_S and the negative parameter of itself $-Z_S$. Fig. 8 shows the equivalent circuit of \mathbf{Y}_{X3} . Assuming the structure of the intrinsic TL is perfectly symmetric, the Y-matrix of the intrinsic TL which length is $\ell_{21} (= \ell_2 - \ell_1)$, $\mathbf{Y}_{TL,\ell_{21}}$, can be expressed by Eq. (4). By using Eq. (6), \mathbf{Y}_{X3} is approximated by Eq. (5). $\text{ytoz}()$ is a transformation function from Y-parameter to Z-parameter.

$$\mathbf{Y}_{TL,\ell_{21}} = \begin{bmatrix} Y_{TL,1,\ell_{21}} & Y_{TL,2,\ell_{21}} \\ Y_{TL,2,\ell_{21}} & Y_{TL,1,\ell_{21}} \end{bmatrix} \quad (4)$$

$$\begin{aligned} \mathbf{Y}_{X3} &= \text{ztoy} \left(\text{ytoz}(\mathbf{Y}_{TL,\ell_{21}}) + \begin{bmatrix} Z_S & 0 \\ 0 & -Z_S \end{bmatrix} \right) \\ &\approx \begin{bmatrix} Y_{TL,1,\ell_{21}} - Z_S(Y_{TL,1,\ell_{21}}^2 - Y_{TL,2,\ell_{21}}^2) & Y_{TL,2,\ell_{21}} \\ Y_{TL,2,\ell_{21}} & Y_{TL,1,\ell_{21}} + Z_S(Y_{TL,1,\ell_{21}}^2 - Y_{TL,2,\ell_{21}}^2) \end{bmatrix} \end{aligned} \quad (5)$$

The following assumption is used.

$$Z_S^2 \ll \frac{1}{Y_{TL,1,\ell_{21}}^2 - Y_{TL,2,\ell_{21}}^2} \quad (6)$$

Therefore, \mathbf{Y}_{X2} can be obtained as the twofold of $\mathbf{Y}_{TL,\ell_{21}}$ as explained in Eq. (7). By the procedure as mentioned above, the Y-parameter matrix of the intrinsic TL $\mathbf{Y}_{TL,\ell_{21}}$ is obtained.

$$\mathbf{Y}_{X2} = \mathbf{Y}_{X3} + \text{Swap}(\mathbf{Y}_{X3})$$

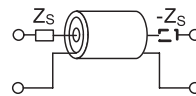


Fig. 8 The equivalent circuit of \mathbf{Y}_{X3} .

$$= \begin{bmatrix} 2Y_{TL,1,\ell_{21}} & 2Y_{TL,2,\ell_{21}} \\ 2Y_{TL,2,\ell_{21}} & 2Y_{TL,1,\ell_{21}} \end{bmatrix} = 2\mathbf{Y}_{TL,\ell_{21}} \quad (7)$$

$\mathbf{Y}_{TL,\ell_{21}}$ can be obtained from $\mathbf{Y}_{TL,\ell_{21}}$ by using Eq. (8).

$$\mathbf{Y}_{TL,\ell_1} = \text{ftoy}(\text{ytof}(\mathbf{Y}_{TL,\ell_{21}}))^n \quad (8)$$

$$\ell_1 = n\ell_{21} \quad (9)$$

This method mentioned above is the same as [8]. For de-embedding of other DUTs such as transistors, capacitors, inductors, etc, the pad parasitics of Z_S and Z_P are derived, which are frequency-dependent parameters. The Y-parameter matrix of the measurement data, \mathbf{Y}_{TL,ℓ_1}^m , of the TL is expressed by \mathbf{Y}_{TL,ℓ_1} in Eq. (10). Z_P is a shunt component at both ports, so it is derived from the Y-parameter matrix.

$$\begin{aligned} \mathbf{Y}_{TL,\ell_1}^m &= \text{ztoy} \left(\text{ytoz}(\mathbf{Y}_{TL,\ell_1}) + \begin{bmatrix} Z_S & 0 \\ 0 & Z_S \end{bmatrix} \right) \\ &+ \begin{bmatrix} \frac{1}{Z_P} & 0 \\ 0 & \frac{1}{Z_P} \end{bmatrix} = \begin{bmatrix} \frac{Z_S + Z'_1}{\Delta Z'^2} + \frac{1}{Z_P} & \frac{Z'_2}{\Delta Z'^2} \\ \frac{Z'_2}{\Delta Z'^2} & \frac{Z_S + Z'_1}{\Delta Z'^2} + \frac{1}{Z_P} \end{bmatrix} \end{aligned} \quad (10)$$

$$\begin{aligned} \Delta Z'^2 &= (Z_S + Z'_1)^2 - Z'^2_2 \\ Z'_1 &= \frac{Y_{TL,1,\ell_1}}{Y_{TL,1,\ell_1}^2 - Y_{TL,2,\ell_1}^2}, \quad Z'_2 = \frac{Y_{TL,2,\ell_1}}{Y_{TL,1,\ell_1}^2 - Y_{TL,2,\ell_1}^2} \end{aligned}$$

The Y-parameter matrix \mathbf{Y}_{X4} is defined as expressed in Eq. (11). If Eq. (13) is satisfied, the shunt parasitic Z_P is obtained by adding $Y(1,1)$ and $Y(1,2)$ of \mathbf{Y}_{X4} as expressed in Eq. (12).

$$\mathbf{Y}_{X4} = \mathbf{Y}_{TL,\ell_1}^m - \mathbf{Y}_{TL,\ell_1} \quad (11)$$

$$Y_{X4,11} + Y_{X4,12} \approx \frac{1}{Z_P} \quad (12)$$

$$\left| \frac{1}{Z_P \cdot (Y_{TL,1,\ell_1} + Y_{TL,2,\ell_1})} \cdot \left(1 + \frac{1}{Z_S \cdot (Y_{TL,1,\ell_1} + Y_{TL,2,\ell_1})} \right) \right| \gg 1 \quad (13)$$

To use the approximations, Eqs. (6) and (13), the parasitic components in the contact pad should be small as compared with the transmission line.

Next, we evaluate the pad series parasitic component Z_S . By subtracting the shunt parasitics from the measurement data of the TL, we can obtain \mathbf{Y}_{X5} that is the parameter of the intrinsic TL with the series parasitic components as expressed in Eq. (14).

$$\mathbf{Y}_{X5} = \mathbf{Y}_{TL}^m - \begin{bmatrix} \frac{1}{Z_P} & 0 \\ 0 & \frac{1}{Z_P} \end{bmatrix} \quad (14)$$

Here, Z_S is derived from Y_{X5} . It is assumed that Y_{X5} expresses a reciprocal and uniform transmission line. The resistance and the inductance per length are defined as $R_{ip}(f)$ and $L_{ip}(f)$, respectively. These value can be calculated from Y_{X5} [13], and the values are frequency dependent. As shown in Fig. 9, the total series resistance $R_i(f)$ and inductance $L_i(f)$ can be expressed by multiplying the line length ℓ_i as follows.

$$L_i(f) = \ell_i L_{ip}(f) \quad (15)$$

$$R_i(f) = \ell_i R_{ip}(f) \quad (16)$$

The following assumption is used (See Appendix).

$$|\gamma \ell_i| \ll 1, \quad (17)$$

where γ is the propagation constant of the transmission line.

This procedure is implemented by using two transmission lines with different length. The values of the calculated inductances are plotted on a graph as shown in Fig. 10(a). Then the line connecting these two points is drawn. The intercept of the line, $L_0(f)$, is the inductance of the series parasitic components of the contact pad because $L_i(f)$ is the only component of the pad when the line length is zero. $L_0(f)$ can be calculated by Eq. (18).

$$L_0(f) = \frac{\ell_2 L_1(f) - \ell_1 L_2(f)}{\ell_2 - \ell_1} \quad (18)$$

In this case, the measurement data of two transmission lines are used. However, by using growing number of transmission lines in different length, the more accurate value of $L_0(f)$ can be obtained. In that case, the offset value can be derived by the method of least squares.

The same procedure is applied to the resistance. The graph of the resistance is shown in Fig. 10(b). $R_0(f)$ can be calculated by Eq. (19).

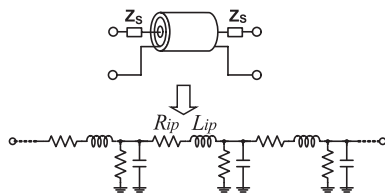


Fig. 9 The resistance and inductance of Y_{X5} .

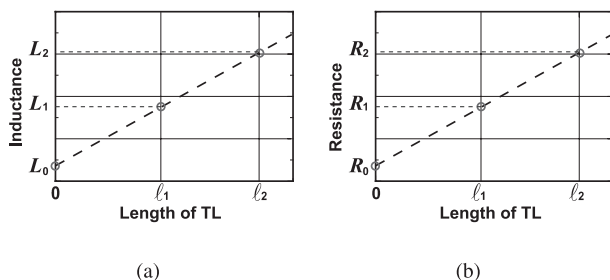


Fig. 10 The graph of total series components. (a) Inductances. (b) Resistances.

$$R_0(f) = \frac{\ell_2 R_1(f) - \ell_1 R_2(f)}{\ell_2 - \ell_1} \quad (19)$$

The series parasitic components of the pad, Z_S , is defined by the following equation.

$$Z_S = \frac{1}{2} \cdot (R_0(f) + j\omega L_0(f)) \quad (20)$$

The parasitic components, Z_S and Z_P , can be obtained by Eq. (20) and Eq. (12). This pad model can be utilized for the de-embedding of other-DUTs.

4. Experimental Results

The evaluations of the conventional and proposed methods are applied by using the measurement data of transmission lines with different length. Twelve-metal-layer 65 nm CMOS process is used. The structure of transmission lines is a coplanar strip line with a bottom ground as shown in Fig. 11. In this experiment, the lengths of the transmission lines are $200\mu\text{m}$ and $400\mu\text{m}$. Because the probe manufacturer (Cascade Microtech, Inc.) recommends the distance between probes should be more than $200\mu\text{m}$. Besides, if the length is long as compared with the wave length, the $\lambda/4$ resonance occurs and it has effect on the measurement data. The structure and size of the contact pad are shown in Fig. 12. The size of signal pad is minimized as possible, $40\mu\text{m} \times 60\mu\text{m}$, to reduce parasitic inductance and capacitance. Therefore, the pad model can be assumed as lumped parameters as shown in Fig. 5. Fig. 13 shows the chip micrograph of the transmission lines with the contact pads.

Figure 14 shows the calculated results by the proposed and conventional methods. After de-embedding, the characteristic impedance Z_0 is calculated from S-parameter by Eq. (21).

$$Z_0^2 = Z_{nom}^2 \frac{(1 + S_{11})^2 - S_{21}^2}{(1 - S_{11})^2 - S_{21}^2} \quad (21)$$

where Z_{nom} represents the normalized impedance, and it is 50Ω in this case. Figure 14(a) shows characteristic impedances of $200\mu\text{m}$ -long and $400\mu\text{m}$ -long transmission lines, which are de-embedded by the open-short method. Figure 14(b) shows a result by the thru-only method, and Fig. 14(c) shows a result by the proposed method.

The characteristic impedance should be equal to each

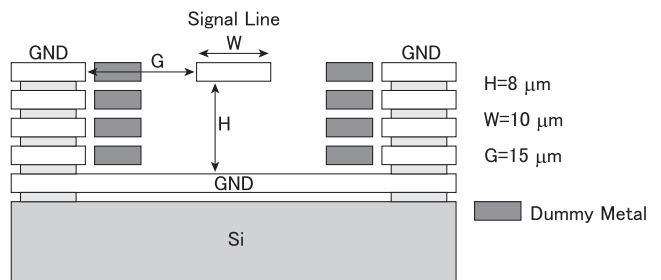


Fig. 11 The structure of TL.

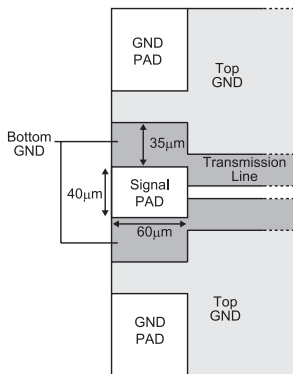


Fig. 12 The structure of pad.

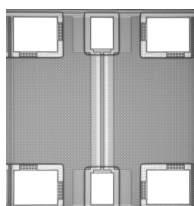


Fig. 13 The chip micrograph of TL.

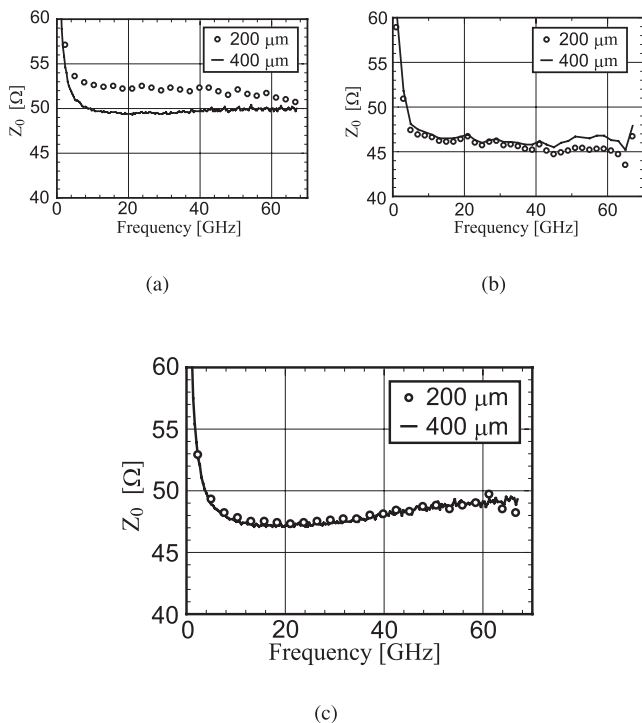


Fig. 14 The calculated result. (a) Open-Short. (b) Thru-only. (c) Proposed.

other even if it is calculated from different-length transmission lines. However, the open-short method and thru-only method have large error in characteristic impedance, which is caused by the error in the de-embedding calculation. In addition, Z_0 calculated by the thru-only method has the variation caused by the measurement error of the thru pattern,

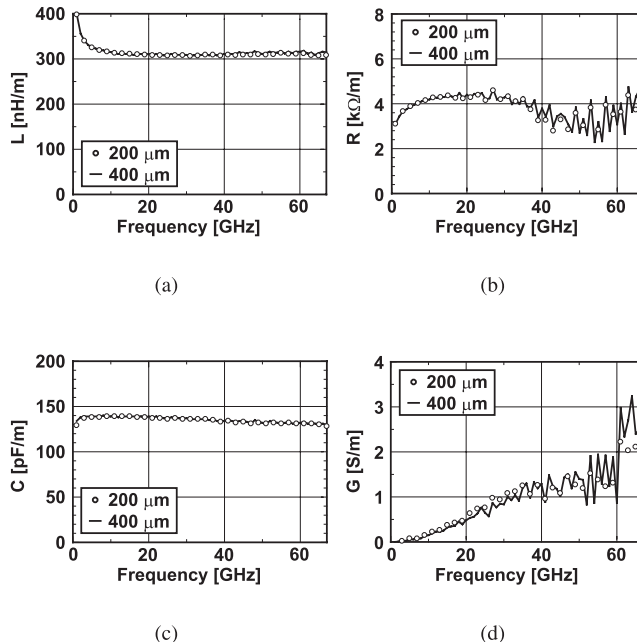


Fig. 15 The values of the transmission line per length. (a) Inductance. (b) Resistance. (c) Capacitance. (d) Conductance.

which is caused by the too short thru pattern, $40 \mu\text{m}$.

Using the proposed method, the characteristic impedances of the transmission lines agree with each other as shown in Fig. 14(c). In the thru-only method, the error between characteristic impedances is 1~4% above 40 GHz. Meanwhile, in the proposed method, the error is less than 0.7%. This result demonstrates the accuracy of the proposed de-embedding method.

The values per length of the transmission lines calculated from $Y_{TL,\ell_{21}}$ are shown in Fig. 15. Figure 16 shows the pad parasitics calculated by the proposed method. Figures 16(a)(c) show the series inductance and the shunt capacitance, and they are almost constant with frequency. The inductance is about 13 pH, and the capacitance is about 20 fF. Figures 16(b)(d) show the series resistance and the shunt conductance, and they increase with frequency because of skin effect and frequency-dependence of dielectric loss. The value of R_0 is unstable around 60 GHz. The reason is that the measurement of resistance is difficult at high frequency. However the inductance and the capacitance are dominant at high frequencies, so the error in R_0 is not so important.

The extracted values shown in Fig. 16 are reasonable according to the actual structure of the contact pad, and approximate values can be calculated as follows. By calculating from the value of intrinsic transmission line, the inductance of $30 \mu\text{m}$ -length transmission line is about 9 pH. The half length of the contact pad is $30 \mu\text{m}$, so we can expect that its inductance is nearly 9 pH. If the probes are put on center of the contact pads, the DC resistance of the contact pad is about 0.1Ω . It is nearly equal to the value of R_0 . Calculating from process parameters, the capacitance of the

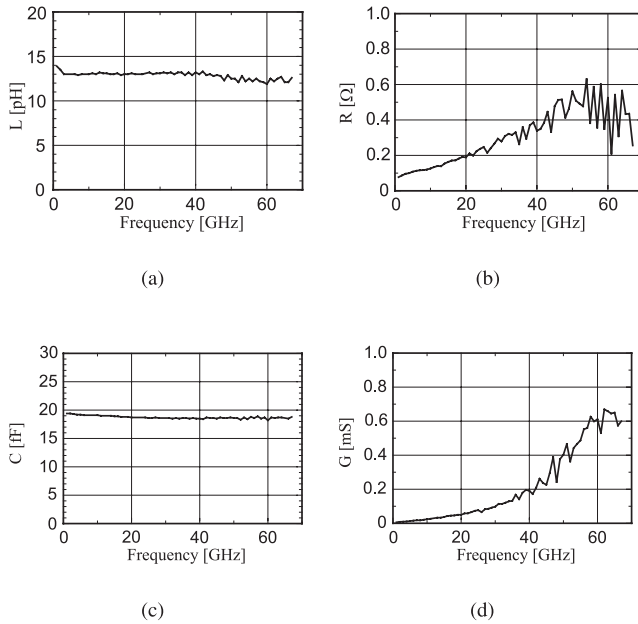


Fig. 16 The pad parasitics calculated by the proposed method. (a) Series inductance. (b) Series resistance. (c) Shunt capacitance. (d) Shunt conductance.

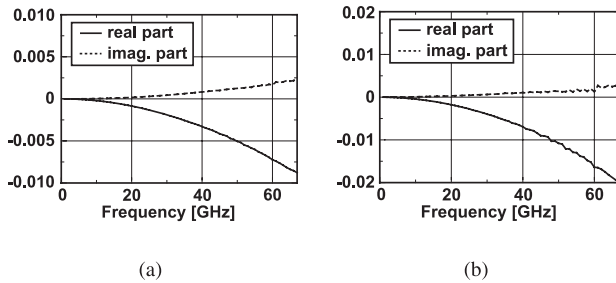


Fig. 17 The left terms in (a) Eq. (22) and (b) Eq. (23).

contact pad is about 11 fF. There are dummy metals under the contact pad, so 19 fF of C_0 is a reasonable value. The tangent-delta values calculated from the transmission line and the pad model are 0.04 and 0.08, respectively.

In this way, the pad model can be built and be also applied for de-embedding other DUTs, e.g., transistors, capacitors, etc.

Next, the effect of the approximation, Eqs. (6) and (13), in the proposed method is discussed. Equations (6) and (13) can be converted to Eqs. (22) and (23), respectively. The real and imaginary parts in the left terms in Eqs. (22) and (23) are shown in Fig. 17.

$$\left| \frac{Z_S^2}{Z_0^2} \right| \ll 1 \quad (22)$$

$$\left| \frac{Z_S \cdot Z_P \cdot (Y_{TL,1,\ell_1} + Y_{TL,2,\ell_1})^2}{1 + Z_S \cdot (Y_{TL,1,\ell_1} + Y_{TL,2,\ell_1})} \right| \ll 1 \quad (23)$$

The absolute values of the real and imaginary parts are less than 0.02 among the entire frequency. Thus, the approximation is valid in this case.

5. Conclusion

A new de-embedding method using two long lines is proposed. Using this method, the accurate de-embedding is realized, and it can be applied to transistors, capacitors, etc as well as transmission lines. The proposed de-embedding method is accurate even at mm-wave frequencies because it does not utilize the open- and short-patterns and the short thru pattern used in the conventional methods. The conventional de-embedding patterns cause the de-embedding error at mm-wave frequencies. The de-embedding of the transmission lines is demonstrated. In the experimental results, the error in characteristic impedance between the different-length transmission lines is less than 0.7% above 40 GHz for the proposed method while two conventional methods have larger error.

Acknowledgement

This work was supported by MIC, NEDO, STARC, VLSI Design and Education Center (VDEC), the University of Tokyo in collaboration with Cadence Design Systems and Agilent Technologies Japan, Ltd. and Fujitsu Laboratories Ltd., Japan.

References

- [1] A. Parsa and B. Razavi, "A 60 GHz CMOS receiver using a 30 GHz LO," IEEE International Solid-State Circuits Conference Digest of Technical Papers, pp.190–191.606, Feb. 2008.
- [2] J.F. Buckwalter and J. Kim, "A 26 dB-gain 100 GHz Si/SiGe cascaded constructive-wave amplifier," IEEE International Solid-State Circuits Conference Digest of Technical Papers, pp.488–489, Feb. 2009.
- [3] Y. Hamada, M. Tanomura, M. Ito, and K. Maruhashi, "A high gain 77 GHz power amplifier operating at 0.7V based on 90 nm CMOS technology," IEEE Microwave and Wireless Components Letters, vol.19, no.5, pp.329–331, May 2009.
- [4] P.J.V. Wijnen, H.R. Claessen, and E.A. Wolsheimer, "A new straightforward calibration and correction procedure for "on-wafer" high frequency s-parameter measurements (45 MHz-18 GHz)," Proc. Bipolar/BiCMOS Circuits and Technology Meeting, pp.70–73, Sept. 1987.
- [5] L.F. Tiemeijer, R.J. Havens, A.B.M. Jansman, and Y. Bouttement, "Comparison of the "pad-open-short" and "open-short-load" deembedding techniques for accurate on-wafer RF characterization of high-quality passives," IEEE Trans. Microw. Theory Tech., vol.53, no.2, pp.723–729, Feb. 2005.
- [6] M. Koelen, J. Geelen, and M. Versleijen, "An improved de-embedding technique for on-wafer high-frequency characterization," Proc. Bipolar/BiCMOS Circuits and Technology Meeting, pp.188–191, Sept. 1991.
- [7] H. Ito and K. Masu, "A simple through only de embedding method for on wafer s parameter measurements up to 110 GHz," IEEE MTT-S Int. Microw. Symp. Dig., pp.383–386, June 2008.
- [8] A.M. Mangan, S.P. Voinescu, M.T. Yang, and M. Tazlauanu, "De-embedding transmission line measurements for accurate modeling of IC designs," IEEE Trans. Electron Devices, vol.53, no.2, pp.235–241, Feb. 2006.
- [9] J. Song, F. Ling, G. Flynn, W. Blood, and E. Demircan, "A de-embedding technique for interconnects," Electrical Performance of

Electronic Packaging, pp.129–132, Oct. 2001.

- [10] L. Hayden, "Calibration errors when neglecting crosstalk," Proc. ARFTG Microwave Measurements Conference, Dec. 2005.
- [11] N. Li, K. Matsushita, N. Takayama, S. Ito, K. Okada, and A. Matsuzawa, "Evaluation of a multi-line de-embedding technique up to 110 GHz for millimeter-wave CMOS circuit design," IEICE Trans. Fundamentals, vol.E93-A, no.2, pp.431–439, Feb. 2010.
- [12] N. Takayama, K. Matsushita, S. Ito, N. Li, K. Bunsen, K. Okada, and A. Matsuzawa, "A multi-line de-embedding technique for mm-wave CMOS circuits," Proc. IEEE Asia Pacific Microwave Conference, Dec. 2009.
- [13] W.R. Eisenstadt and Y. Eo, "S-parameter-based IC interconnect transmission line characterization," IEEE Trans. Components and Manufacturing Technology, vol.15, no.4, pp.483–490, 1992.

Appendix

In this appendix, it is shown that the series parasitic impedance Z_S can be calculated from the series impedance per length $Z_0\gamma$.

The Z-parameter of ℓ_i -length transmission line is defined as \mathbf{Z}_{TL,ℓ_i} . \mathbf{Z}_{TL,ℓ_i} is expressed as shown in Eq. (A·1).

$$\mathbf{Z}_{TL,\ell_i} = \text{ytoz}(\mathbf{Y}_{TL,\ell_i})$$

$$= \begin{bmatrix} \frac{Y_{TL,1,\ell_i}}{Y_{TL,1,\ell_i}^2 - Y_{TL,2,\ell_i}^2} & \frac{-Y_{TL,2,\ell_i}}{Y_{TL,1,\ell_i}^2 - Y_{TL,2,\ell_i}^2} \\ \frac{-Y_{TL,2,\ell_i}}{Y_{TL,1,\ell_i}^2 - Y_{TL,2,\ell_i}^2} & \frac{Y_{TL,1,\ell_i}}{Y_{TL,1,\ell_i}^2 - Y_{TL,2,\ell_i}^2} \end{bmatrix} \quad (\text{A}\cdot 1)$$

$$= \begin{bmatrix} A & B \\ B & A \end{bmatrix}, \quad (\text{A}\cdot 2)$$

where A and B are defined as follows.

$$A = \frac{Y_{TL,1,\ell_i}}{Y_{TL,1,\ell_i}^2 - Y_{TL,2,\ell_i}^2} = \frac{Z_0 \cosh(\gamma\ell_i)}{\sinh(\gamma\ell_i)} \quad (\text{A}\cdot 3)$$

$$B = \frac{-Y_{TL,2,\ell_i}}{Y_{TL,1,\ell_i}^2 - Y_{TL,2,\ell_i}^2} = \frac{Z_0}{\sinh(\gamma\ell_i)} \quad (\text{A}\cdot 4)$$

The characteristic impedance Z_0 and the propagation constant γ are expressed by using A and B [13].

$$Z_0^2 = A^2 - B^2 \quad (\text{A}\cdot 5)$$

$$e^{\gamma\ell_i} = \frac{A}{B} + \frac{\sqrt{A^2 - B^2}}{B} \quad (\text{A}\cdot 6)$$

In addition, the resistance $R_{ip}(f)$ and the inductance $L_{ip}(f)$ per length are expressed by the following equations.

$$L_{ip}(f) = \frac{\text{Im}[Z_0\gamma]}{2\pi f} \quad (\text{A}\cdot 7)$$

$$R_{ip}(f) = \text{Re}[Z_0\gamma] \quad (\text{A}\cdot 8)$$

Next, the influence of the series parasitic impedance Z_S is calculated. The total series impedance is expressed by $Z_0\gamma\ell_i$, and the difference by Z_S is defined as $\Delta(Z_0\gamma\ell_i)$. In this case, the term A becomes $A + Z_S$. The difference can be expressed by the sum of the differences of Z_0 and $\gamma\ell_i$ as

follows.

$$\frac{\Delta(Z_0\gamma\ell_i)}{Z_0\gamma\ell_i} = \frac{\Delta Z_0}{Z_0} + \frac{\Delta(\gamma\ell_i)}{\gamma\ell_i} \quad (\text{A}\cdot 9)$$

Here, $\Delta Z_0/Z_0$ can be obtained by the following equations.

$$\frac{\Delta Z_0}{Z_0} = \frac{\sqrt{(A + Z_S)^2 - B^2} - \sqrt{A^2 - B^2}}{Z_0}$$

$$= \sqrt{1 + \frac{2AZ_S}{Z_0^2} + \frac{Z_S^2}{Z_0^2}} - 1 \quad (\text{A}\cdot 10)$$

$$\approx \frac{AZ_S}{Z_0^2} = \frac{Z_S}{Z_0 \tanh(\gamma\ell_i)} \quad (\text{A}\cdot 11)$$

where the following assumption is used.

$$\left| \frac{Z_S^2}{Z_0^2} \right| \ll 1 \quad (\text{A}\cdot 12)$$

Then, the difference of $\Delta(\gamma\ell_i)$ is calculated as follows.

$$\frac{\Delta(\gamma\ell_i)}{\gamma\ell_i} = \frac{\ln X' - \ln X}{\ln X}$$

$$= \frac{\ln \frac{X'}{X}}{\ln X}, \quad (\text{A}\cdot 13)$$

where X and X' are defined as follows.

$$X = e^{\gamma\ell_i} = \frac{A}{B} + \frac{\sqrt{A^2 - B^2}}{B} \quad (\text{A}\cdot 14)$$

$$X' = e^{\gamma'\ell_i} = \frac{A + Z_S}{B} + \frac{\sqrt{(A + Z_S)^2 - B^2}}{B} \quad (\text{A}\cdot 15)$$

The difference of $\Delta(\gamma\ell_i)/(\gamma\ell_i)$ can be calculated by the following equations.

$$\frac{X'}{X} = \frac{A + Z_S + \sqrt{(A + Z_S)^2 - B^2}}{A + \sqrt{A^2 - B^2}}$$

$$\approx 1 + \frac{Z_S}{Z_0} \quad (\text{A}\cdot 16)$$

$$\frac{\Delta(\gamma\ell_i)}{\gamma\ell_i} = \frac{\ln \frac{X'}{X}}{\ln X} \quad (\text{A}\cdot 17)$$

$$= \frac{\ln \left(1 + \frac{Z_S}{Z_0} \right)}{\ln X} \quad (\text{A}\cdot 18)$$

$$\approx \frac{Z_S}{Z_0\gamma\ell_i} \quad (\text{A}\cdot 19)$$

From Eqs. (A·9), (A·11) and (A·19), the following equation can be obtained.

$$\Delta(Z_0\gamma\ell_i) = Z_S \left(1 + \frac{\gamma\ell_i}{\tanh(\gamma\ell_i)} \right) \quad (\text{A}\cdot 20)$$

$$\approx 2Z_S, \quad (\text{A}\cdot 21)$$

where the following assumption is used.

$$|\gamma \ell_i| \ll 1. \quad (\text{A}\cdot 22)$$

Under the assumptions Eqs. (A·12) and (A·22), Eq. (A·21) means that the series parasitic impedance Z_S can be derived from the product of the impedance per length $Z_0\gamma$ and the line length ℓ_i .



Naoki Takayama received the B.E. degree in Electrical and Electronic Engineering from Tokyo Institute of Technology, Tokyo, Japan, in 2008. He is currently perusing the M.E. degree in Tokyo Institute of Technology, Tokyo, Japan.



Kota Matsushita received the B.E. degree in Electrical and Electronic Engineering from Tokyo Institute of Technology, Tokyo, Japan, in 2009. He is studying toward the M.E. degree in Department of Physical Electronics, Tokyo Institute of Technology, Tokyo, Japan. His research interests include RF circuit design.



Shogo Ito received the B.E. degree in Electrical and Electronic Engineering from Tokyo Institute of Technology, Tokyo, Japan, in 2008. He is studying toward the M.E. degree in Department of Physical Electronics, Tokyo Institute of Technology, Tokyo, Japan. His research interests include RF circuit design.



Ning Li received the B.S. degree in Electronics Engineering and the M.S. degree in Physical Electronics from Xi'an Jiaotong University, China in 1999 and 2002. In 2002 she joined Department of Electronics and Information Engineering, Xi'an Jiaotong University, Xi'an, China. Currently she is studying for her Ph.D. degree in Tokyo Institute of Technology, Tokyo, Japan.



Keigo Bunsen received the B.E. degree in Electrical and Electronic Engineering from Tokyo Institute of Technology, Tokyo, Japan, in 2009. He is studying toward the M.E. degree in Department of Physical Electronics, Tokyo Institute of Technology, Tokyo, Japan. His research interests include RF circuit design.



Kenichi Okada received the B.E., M.E. and Ph.D. degrees in Communications and Computer Engineering from Kyoto University, Kyoto, Japan, in 1998, 2000, and 2003, respectively. From 2000 to 2003, he was a Research Fellow of the Japan Society for the Promotion of Science in Kyoto University. From 2003 to 2007, he worked as an Assistant Professor at Precision and Intelligence Laboratory, Tokyo Institute of Technology, Yokohama, Japan. Since 2007, he has been an Associate Professor at Department of Physical Electronics, Tokyo Institute of Technology, Tokyo, Japan. He has authored or co-authored more than 150 journal and conference papers. His current research interests include reconfigurable RF CMOS circuits for cognitive radios, 60 GHz CMOS RF frontends, and low-voltage RF circuits. He is a member of IEEE, the Information Processing Society of Japan (IPJS), and the Japan Society of Applied Physics (JSAP).



Akira Matsuzawa received B.S., M.S., and Ph.D. degrees in electronics engineering from Tohoku University, Sendai, Japan, in 1976, 1978, and 1997 respectively. In 1978, he joined Matsushita Electric Industrial Co. Ltd. Since then, he has been working on research and development of analog and Mixed Signal LSI technologies; ultra-high speed ADCs, intelligent CMOS sensors, RF CMOS circuits, digital read-channel technologies for DVD systems, ultra-high speed interface technologies for metal and optical fibers, a boundary scan technology, and CAD technology. He was also responsible for the development of low power LSI technology, ASIC libraries, analog CMOS devices, SOI devices. From 1997 to 2003, he was a general manager in advanced LSI technology development center. On April 2003, he joined Tokyo Institute of Technology and he is a professor on physical electronics. Currently he is researching in mixed signal technologies; CMOS wireless transceiver, RF CMOS circuit design, data converters, and organic EL drivers. He served the guest editor in chief for special issue on analog LSI technology of IEICE transactions on electronics in 1992, 1997, and 2003, the vice-program chairman for International Conference on Solid State Devices and Materials (SSDM) in 1999 and 2000, the Co-Chairman for Low Power Electronics Workshop in 1995, a member of program committee for analog technology in ISSCC and the guest editor for special issues of IEEE Transactions on Electron Devices. He has published 26 technical journal papers and 46 international conference papers. He is co-author of 8 books. He holds 34 registered Japan patents and 65 US and EPC patents. In April 2003 he joined, as an Professor, the Department of Physical electronics at Titech. He received the IR100 award in 1983, the R&D100 award and the remarkable invention award in 1994, and the ISSCC evening panel award in 2003 and 2005. He is an IEEE Fellow since 2002.